The Space-Based Visible Sensor

David C. Harrison and Joseph C. Chow

The Space-Based Visible (SBV) instrument, a small visible-band surveillance sensor built by the Massachusetts Institute of Technology's Lincoln Laboratory, is part of a sensor ensemble on the Midcourse Space Experiment satellite, a Ballistic Missile Defense Organization program. The SBV sensor is designed to perform above-the-horizon surveillance experiments and acquire visible and very-near-infrared band data (450 to 950 nm) on targets and backgrounds. This article describes the flight configuration of the SBV sensor, its incorporated technologies, its preflight status, and the surveillance experiments to be performed.

INTRODUCTION

The Space-Based Visible (SBV) sensor[1] is designed to demonstrate the feasibility and utility of an above-the-horizon surveillance capability from a space platform. It uses a broadband visible wavelength detector and signal processor to automatically detect space objects, such as intercontinental ballistic missile targets and satellites, from their reflected sunlight. The goal of the SBV instrument is to provide high-performance search, detection, tracking, and data gathering on space objects to support both midcourse surveillance and space surveillance missions. The SBV sensor is part of the instrument package on the Midcourse Space Experiment (MSX) spacecraft.[2]

During the MSX flight, the SBV sensor will perform broadband, visible, above-the-horizon surveillance experiments on cooperative intercontinental ballistic missile targets, sounding rocket targets, and satellites to demonstrate midcourse sensor functions and space surveillance capabilities from space. During its operational lifetime, the SBV sensor is designed to acquire a visible-band database on these targets and also on background phenomena such as Earth-limb, aurora, airglow, and celestial phenomena. Finally, the SBV sensor will demonstrate technologies required for a space-based, visible-band, above-the-horizon surveillance sensor.

The SBV sensor uses 420×420 pixel charge-coupled device (CCD) imagers, designed and manufactured at the Massachusetts Institute of Technology's Lincoln Laboratory (MIT/LL), in a 15-cm aperture telescope designed to reduce interference from out-of-field bright sources in order to view objects as close to the Earth-limb as possible. Another primary feature of the SBV hardware is a signal processor that can provide automated detection of nonstellar moving objects, reducing data volume compared with the raw data set supplied by the imager. Other hardware elements provide power conversion and conditioning, experiment control functions, and signal interfaces to the MSX spacecraft.

A significant part of the SBV surveillance experiment is the ground data analysis system, which is designed to help devise experiments, generate appropriate command sequences, and analyze the data returned by the flight hardware. This system, the SBV Processing Operations and Control Center (SPOCC), will be used throughout the SBV program for monitoring the data obtained during the ground tests and for analyzing the flight housekeeping and status data.

Redundancy was designed into the SBV sensor by having independent sets of spacecraft and internal interfaces. Any power and signal type inside the instrument, or at its interfaces, can tolerate a single failure with no loss of sensor performance. The focal plane is not completely redundant; it has been segmented into two independent zones, isolated except for signal ground connections. A focal plane single failure may result in the loss of up to half of the sensor's total field of regard.

SBV SENSOR DESCRIPTION

An overall block diagram of the sensor is shown in Fig. 1. The sensor is located in two zones: The telescope and focal plane assembly, the telescope aperture cover and controller, and the analog processing electronics are located in the forward section ($+x$ direction) of the spacecraft called the instrument section. The signal processor, experiment controller, power conditioner, and telemetry interface to the spacecraft are in a single assembly, the electronics side assembly, which is located in the aft section ($-x$ direction) of the spacecraft. Figure 2 shows the relative locations of the SBV elements.

Telescope

The telescope was developed for MIT/LL by SSG, Inc., of Waltham, Massachusetts.[3] It employs a three-mirror anastigmat and off-axis reimaging design, as shown in Fig. 3, to maximize stray-light rejection of bright sources such as the sunlit Earth, which may be just outside the field of view (FOV). This design configuration introduces well-defined spatial distortions, a trade-off for good focusing characteristics.

The telescope has three powered optics: a primary mirror, a secondary mirror, and a tertiary mirror. An image is formed between the secondary and tertiary mirrors, and a field stop is placed here to eliminate direct stray light outside the FOV. A fold flat is used to simplify the focal plane packaging and to provide some additional radiation shielding. A Lyot stop is placed just in front of the fold flat, at the image of the entrance aperture, to eliminate stray light diffracted from the aperture. The total FOV of the telescope, including distortions, is about $1.4 \times 6.6°$ with four CCDs in the focal plane. Each pixel has a near-square FOV of about 60 μrad on a side; local distortions vary the size of the pixel FOV from the nominal. An aperture cover, which can be opened and closed on command, is used for contamination control, preventing dirt accumulation during launch and on orbit when the SBV sensor is not being used. The cover has a secondary mechanism that can permanently open the cover if the normal mechanism fails.

Focus quality and stability became an issue early when the initial Hubble results were made known just before the SBV sensor's critical design review. To maintain focus independent of operating temperature, the telescope housing and mirrors were all made of the same type of aluminum, resulting in an athermal system. All elements expand or shrink at the same rate, keeping the focal plane in a fixed location. Plate scale and distortion maps were expected to change with temperature, and computer modeling indicated that it was important to keep temperature gradients low, making athermal assumptions valid. Thick walls, thick mirrors,

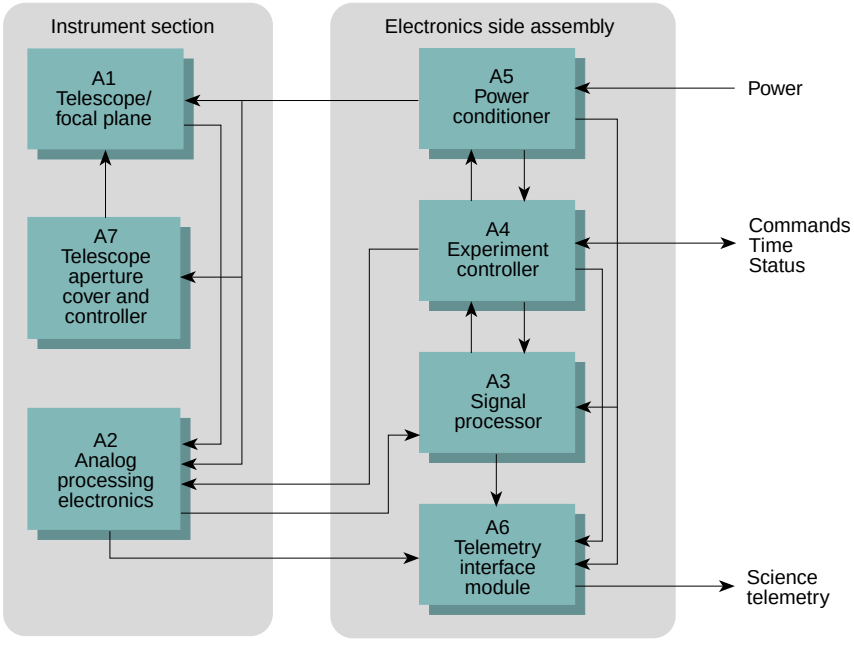

Figure 1. Block diagram of the SBV sensor.

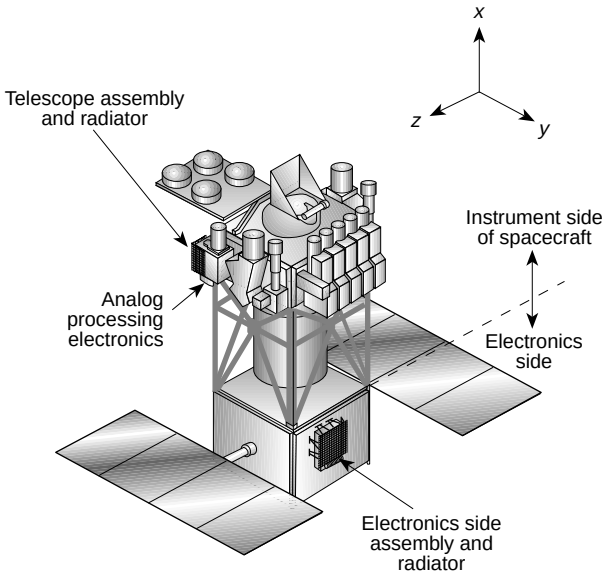

Figure 2. Mounting locations for the SBV sensor units on the MSX spacecraft.

thermal isolation from the spacecraft mounting surface, and a multilayer insulation blanket were incorporated to keep gradients well below the design-allowable value of 3.5°C. Focus is specified as an ensquared energy percentage, which is the percent of total energy in the central pixel after optimum centering, rather than as a modulation transfer function, because the objects to be detected are effectively point sources. The ensquared energy limit was set to be no less than 50% to maximize detection probability and no more than 80% to allow ground analysis of star centroids for subpixel pointing determination by slight oversampling of point sources.

A significant challenge for the SBV program is to keep the telescope optics clean up to, during, and after launch. The first two mirrors are superpolished with gold surfaces to maintain low-scatter characteristics. Our process to maintain cleanliness covers three areas: design, handling, and operation. The design of the telescope eliminated penetrating holes inside the optical cavity. All fasteners were precision-cleaned and then treated to minimize hydrocarbon lubricants by placing a small amount of low-outgassing oil on screw threads to prevent galling. Unlubricated fasteners were found to generate significant amounts of particulate contamination, a serious problem for the SBV sensor. On the ground, the telescope aperture cover is opened only in a class 100 clean tent or a vacuum chamber. A continuous dry nitrogen purge is used, even during shipping, until just before launch. On orbit, the cover will be closed when the sensor is not taking data. A bidirectional reflectance distribution function (BRDF) monitoring lamp is built into the baffle assembly to monitor the BRDF (a good measure of cleanliness) of the primary mirror during thermal-vacuum testing and on orbit.

Focal Plane

The SBV focal plane comprises a 1×4 array of MIT/LL CCID7 frame-transfer visible-light CCDs, which were specifically developed for space surveillance. CCID7 is the design file name, which is an acronym for charge-coupled imaging device 7. The CCD imagers are mounted on a ceramic substrate for electrical interconnections, and the substrate is then bonded to a Kovar tray. The temperature of the focal plane is controlled by a thermoelectric cooler. The focal plane is read out in a sequential mode, one imager at a time, at a pixel rate of 0.5 MHz. This design choice was made by balancing power, mass, and telemetry allocations against data requirements. Each single observation sequence requires that a full frame set be taken using a single CCD before switching to the next CCD for data acquisition. The focal plane wiring is designed to prevent a single CCD failure from affecting more than half of the focal plane; any single failure allows the two imagers on the other half of the focal plane to continue to operate normally.

A primary reason for selecting the CCID7 imager is its unique combination of high charge transfer efficiency and low readout noise. Small charge packets (about four electrons) have been transferred through nearly 1300 pixels of a CCID7 imager with no detectable loss and with no background charge. A charge transfer efficiency of more than 0.99999 allows imaging that preserves over 99% of an initial charge packet generated at the corner of the CCD farthest from the readout node.

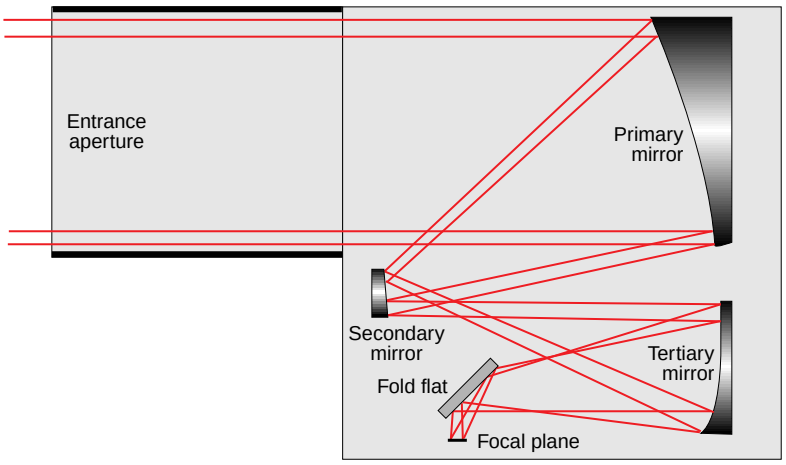

Figure 3. Optical layout of the SBV telescope.

When combined with a linear output node that has less than a six-electron noise floor, the imager can detect a 36-electron charge packet with 95% confidence.

A block diagram of a single CCID7 imager is shown in Fig. 4. The CCID7 layout was designed for three-side butting such that $2 \times N$ focal plane arrays, where N can be any integer, could ultimately be built.[4] Each CCID7 visible imager has a 420×422 pixel imaging area and a 420×422 pixel storage area. The additional two lines in the image and storage areas allow some aluminum light shield misalignment and reduce red diffusion effects of charge into the top of the storage area. All registers have three-phase polysilicon clocks, indicated as P1, P2, and P3 in Fig. 4. The pixel's three-phase polysilicon on nitride clock structure[5] provides high yield and high charge transfer efficiency, and it is relatively insensitive to bias levels. The serial register is extended by 4 pixels to separate the output charge sensing node from the main array, for ease of location, and to provide room for grounds around the output.

Another advantage of the polysilicon on nitride gate construction is that biases are not critical; voltages can be off by 1 or 2 V with virtually no performance change in the imager. Clock voltages are selected to adapt to the charge dynamic range desired and to put the surface into inversion during integration. Biases are carefully filtered to prevent noise injection.

The output node of the CCD is a buried-channel field effect transistor with small geometry that operates as a source follower with a sense node capacitance of about 15 femtofarads. A Siliconix U309 junction field effect transistor buffers the video from the focal plane to the subsequent electronics. The buried-channel field effect transistor and the U309 share the same drain bias, the output drain in Fig. 4.

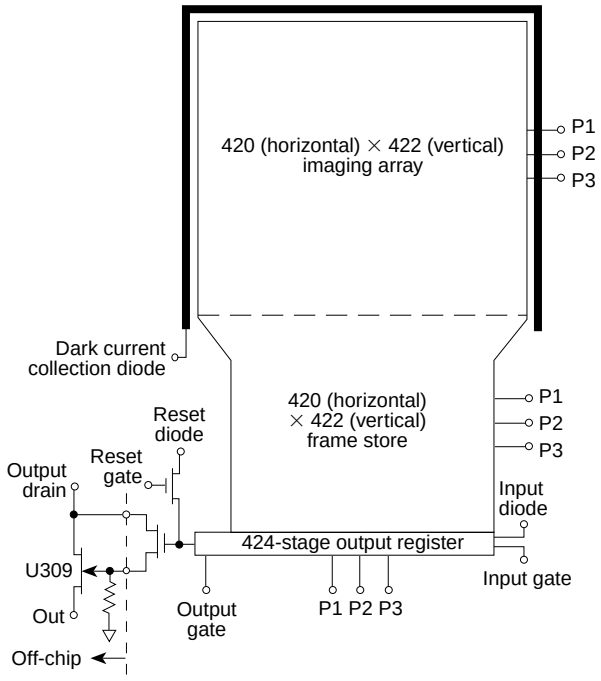

Figure 4. Block diagram of the CCID7 CCD imager. P1, P2, and P3 are three-phase polysilicon clocks.

The CCDs are cooled both actively and passively. Waste heat is radiated to space by a radiator on, but thermally isolated from, the telescope body. The radiator is maintained at a minimum temperature of −43°C by survival heaters. The maximum radiator temperature is expected to be +20°C after some long-duration space surveillance experiments. A thermoelectric cooler is attached to the focal plane Kovar tray through a flexible multilayer aluminum strap. The thermoelectric cooler is driven by an electronics servo system to maintain a maximum −40°C temperature during operation. At this low temperature, dark current is on the order of 18 electrons per pixel per second. The focal plane assembly has been subjected to environmental testing with no detectable change in focal plane performance. Table 1 shows the primary specifications of the CCID7 imager.

CCD Camera

The CCD camera comprises the analog signal processor and a focal plane electronics card located in the telescope near the focal plane. The camera functions were split to place the low-noise electronics near the focal plane for better performance, while removing the higher power processing electronics to a separate assembly, relieving some of the thermal requirements on the telescope.

The CCD camera selects the operating CCD, generates CCD focal plane clocks and biases, coordinates timing with the other SBV elements, and provides a low-noise 12-bit digitized readout. The camera uses a fully redundant, dual-channel architecture for fault tolerance, where only one channel is powered at a time. The camera has two commandable gains and up to five different integration times. The gains are nominally set to provide 6 and 25 electrons per least significant bit of the 12-bit analog-to-digital converters for full-scale responses of about 24,000 and 100,000 electrons, respectively. Two internally timed integration times, 0.4 and 1.6 s, are used during space surveillance operations, and three others, 0.625, 1.000, and 3.125 s, are used for target track and background phenomena measurements, requiring active science telemetry to operate. The camera can gate its output and synchronize to an external pulse, allowing accurate precise time tagging of space surveillance integration times. The pixel rate out of the camera is 0.5 Mpixel/s. Each of the four CCD imagers operates simultaneously, but only one is commanded as a data source.

Table 1. CCID7 imager specifications.

Parameter	Specification
Array size	420 × 422 pixel imaging area
	420 × 422 pixel storage area
Imaging area	11.34 × 11.39 mm, 129.2 mm^2
Pixel size	27 × 27 μm imaging area
	24 × 18 μm storage area
Quantum efficiency	0.28, average over solar spectrum
Clock rate	0.5-MHz nominal serial clocks
Charge transfer efficiency	>0.99999
Output amplifier gain	11-μV/electron, nominal
Operating temperature	−90 to +40°C
	−40°C, nominal operating
Output amplifier noise	<6 electrons rms at −40°C
Full well capacity	>1 × 10^5 electrons, >1.1 V out
Read time	372 ms, nominal
Dark current	<100 electrons/pixel·s at −40°C

Signal Processor

The signal processor algorithm[6] was under development for several years prior to the start of the SBV program. The signal processor hardware[7] can accept from 2 to 16 data frames from the camera, where each frame consists of about 2 Mbits of information. Using this data, the signal processor automatically detects targets and reduces the data flow to a few kilobits per frame set, effectively making a data compression ratio of greater than 1000:1. The signal processor has two redundant channels, each of which uses a Motorola DSP56001 digital signal processor operating at 20 MHz as its processing engine. The algorithmic core of the signal processor is centered around an assumed velocity filter that employs maximum likelihood estimation for clutter rejection and automatic target detection. A 1-bit binary implementation of this algorithm is used to reduce the computational load while maintaining as much performance as possible of a full 12-bit binary assumed velocity filter. The signal processor algorithm normally operates with the spacecraft stabilized in inertial space, where the stars are stationary and the images of moving objects form streaks in the focal plane. This mode is referred to as sidereal track. The signal processor automatically detects these streaks and generates target reports consisting of position and velocity estimates in focal plane coordinates. A target signature, using the 12-bit camera information, can also be included in the target report if commanded. The signal processor can also save a commandable number of the brightest stars' 12-bit data for telemetering to the ground. The star data will be used to refine the pointing knowledge of the SBV sensor to about one-third of a pixel (20 μrad). The pointing algorithms in SPOCC have been validated by ground observations of stars using a telescope and focal plane similar to those in the SBV sensor.

The detection algorithm is run in two stages. While the camera is transmitting data, the signal processor has a real-time stage. Data are stored in three arrays: (1) an average of all frames, (2) the peak value of the frame set, and (3) the second highest value of the frame set. Frame number of occurrence is stored along with the values in the peak and second peak arrays. When the data set is completed, the signal processor enters its second stage, where stars are selected and the main part of the detection algorithm is run. Data from the second highest value is used to estimate the variance of a pixel. After subtracting the average frame data from the peak data, the result is divided by the variance estimate array. This new array has higher values for pixels that saw a changing scene during the frame set, corresponding to anything that had motion relative to the stars. The values are assigned a threshold, providing the single-bit array for the detection process.

The signal processor can also operate when tracking an object, or out of sidereal track, in which the target of interest is tracked and the stars form streaks. This mode requires an accurate knowledge of the angular velocity of the spacecraft, which is furnished by the spacecraft attitude processor, to compensate for the apparent angular velocity of the stars. The algorithm converts the input data to an apparent sidereal track and then operates in its normal mode.

Support Electronics

The support electronics comprise an experiment controller, a power subsystem, and a telemetry interface module. The experiment controller is based on a micropackaged data and control system (μDACS), which is a Harris 80RH86 microprocessor-based computer with a high degree of fault tolerance and error correction (SCI, Inc., Huntsville, Alabama). All control busses are triply redundant with majority logic, and the address and data busses have single-bit error correction syndrome bits. The bus redundancy and error correction allow the μDACS to operate with no loss of speed,

functionality, or capacity after the failure of any internal signal line. The experiment controller is used to read commands uplinked from the ground through the MSX spacecraft and to convert them to the set of commands to operate the SBV sensor. Under ground command, it is used to configure all the other redundant electrical units of the SBV sensor by power and signal switching and to provide health and status messages to the telemetry. Memory inside the experiment controller permits storage of many signal processor results, allowing the SBV sensor to gather and store observation results using neither the MSX tape recorders nor contact with a ground station. When the spacecraft is over a ground receiving site, the MSX telemetry system relays the stored data to the ground.

The power subsystem was built for MIT/LL by Gulton Data Systems, Albuquerque, New Mexico. It provides conditioned, isolated, secondary power for all units except the experiment controller, which has an internal power conditioner. It also switches primary and secondary power with commands from the experiment controller for fault recovery.

The telemetry interface module is a first-in, first-out unit capable of running up to the maximum instantaneous bit rate of 25 Mbits/s. It is used to interleave the SBV telemetry into the spacecraft telemetry stream and interfaces to a redundant spacecraft telemetry system with a complete, independent, interface circuit assigned to each spacecraft system. The high bit rates used in the telemetry system would have made a cross-strapping scheme large and power hungry, inconsistent with the weight and power budgets for the SBV sensor. The telemetry interface module was designed and built at MIT/LL.

Sensor Performance

Since the SBV sensor was designed as a wide-area search sensor pointed by moving the whole satellite, it is subject to the constraint of spacecraft pointing agility. The sensor has a large total FOV of 1.4 × 6.6° (all four CCDs) with a pixel FOV of 60 × 60 μrad. For better metric estimation of a target in angular space, the point-spread function of the telescope is moderately oversampled by the CCD focal plane. The goal is to interpolate the target position to about one-third of a pixel, or 20 μrad.

The instrument is designed to detect as weak a target as possible under a variety of conditions, bounded on one extreme by low-altitude surveillance for which nonrejected Earth radiance (NRER) dominates as background noise and, on the other extreme, by observing targets against a deep space background for which the sensor is nearly internal noise limited.

Table 2 lists these bounding detection sensitivity goals for a signal-to-noise ratio of 6 in both target track and step–stare modes of operation. Detection sensitivity is listed in two ways: (1) target visual magnitude (Vm) and (2) target reflectivity-area product (ρA) referenced to a specular (isotropic) sphere.

CALIBRATION AND TESTING

Integration, test, and calibration are complete, and the SBV sensor is now mounted on the MSX spacecraft.[8] A complete-system thermal vacuum test was run prior to spacecraft integration, simulating the worst-case orbital environments predicted for MSX. The first verifications to come out of integration and testing were that the SBV sensor met its weight and power budgets, as summarized in Table 3. The weight budget was met by careful configuration management. Measured power was lower than predicted because maximum powers were carried for each element in the budget; as usual, actual power requirements for the semiconductors were closer to typical than to the maximum limit. Electrical and mechanical integration were uneventful. Calibration required a long time, which gave us confidence in the stability of the design and component quality.

Electrical Integration

All of the electronic units were tested for functionality and adherence to an internal interface control document generated early in the SBV program. Software testing was performed by running simulated

Table 2. SBV sensor detection sensitivity goals.

Mode of operation	Background	Range (km)	Vm[a]	ρA[b]
Target track,	Low altitude[c]	6,000	12.4	0.10
1.0-s exposure	Deep space[d]	36,000	14.6	0.46
Sidereal,	Low altitude	6,000[e]	11.0	0.35
0.4-s exposure	Deep space	36,000[f]	13.3	1.51

[a]Vm is equivalent visual magnitude brightness.

[b]ρA is reflectivity-area product in square meters.

[c]Non-rejected Earth radiance = 4.2×10^5 W/cm^2·sr at 100-km tangent height.

[d]Celestial background = 2×10^{-10} W/cm^2·sr.

[e]Target angular velocity = 75 arcsec/s.

[f]Target angular velocity = 15 arcsec/s.

Table 3. Weight and power of the SBV sensor.

Quantity	ICD budget[a]	Measured
Mass	79 kg	78 kg
Operating power	98 W	64 W
Heater power	55 W	45 W

[a]Interface control document (ICD) budget is the maximum allowed for the SBV sensor by the MSX spacecraft.

observing sequences under all possible conditions. Here, a brassboard system, electrically identical to the flight unit, served as a test bed for software verification without requiring clean room access, speeding up the process and providing deeper probing into potential problems through connected ground support equipment. A ground support equipment test port was placed on the SBV flight hardware for monitoring points inside the electronics without opening any interface connections. The test port allowed external checking of the digital camera data stream, a signal processor status message, the low-rate science telemetry, and the experiment controller. Of these functions, the camera data and experiment controller monitors were used most during system testing. Camera data were displayed independently on a ground support equipment system during integration and testing, permitting the operator to see an image at all times that the camera was running, verifying that the imagers were operating properly.

Of greater utility, especially during software development, was the ground support equipment test port of the experiment controller. This port comprised a data-logging monitor that could mirror serial messages received or generated by the experiment controller and a control function that could permit the ground support equipment to take over the experiment controller's central processor unit for rapid tests of software and bug fixes. The data-logging monitor of the ground support equipment test port was used extensively during spacecraft integration, validating all spacecraft serial communications.

The instrument integration was expedited by close auditing against both the spacecraft interface control document and an internal interface control document generated at Lincoln Laboratory. A set of engineering units, identical electrically and mechanically to the flight hardware, was used as a pathfinder for early verification of all internal and spacecraft interfaces.

Calibration

The calibration efforts concentrated on the telescope and focal plane. Measurements verified early that the electronics had insignificant effects on system calibration compared with calibration source stabilities and equipment setup repeatability. An engineering model of the electronics was interchanged with the flight electronics with no detectable changes. Figure 5 shows a cutaway drawing of the telescope and a field-of-regard view in

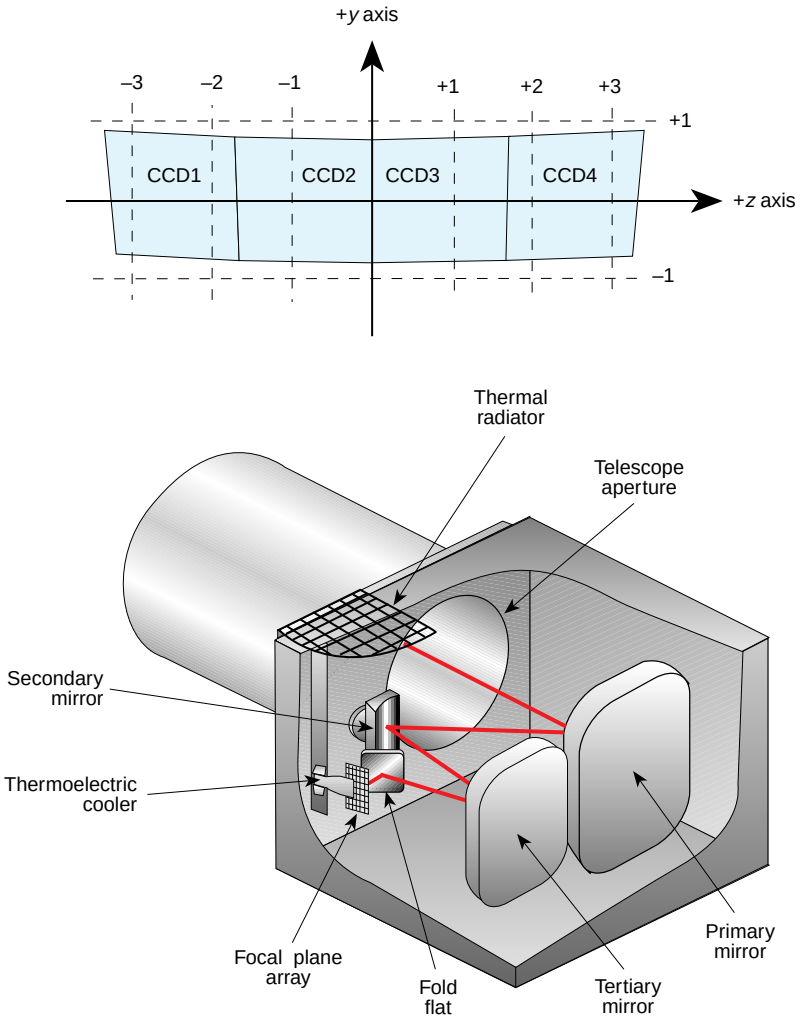

Figure 5. SBV telescope and focal plane projection. This all-aluminum instrument employs an off-axis reimaging design and is thermally isolated. It can accommodate four MIT/LL CCID7 imagers with the following specifications: 15-cm *f*/3, 1.5 × 6.6° FOV, 60-μrad resolution, and >60% ensquared energy. The telescope was developed by SSG, Inc., of Waltham, Massachusetts.

spacecraft coordinates. The telescope has a distorted field of regard, a trade-off made against focus quality and design time. The distortion requirement was driven by the signal processor; to maintain a high probability of detection, any straight line in space projected onto the focal plane would have no more than 0.2-pixel deviation from a straight line over a 100-pixel length. Focus quality and radiometric calibration were also critical measurements. Table 4 shows the primary calibration parameters and their requirements.

The ensquared energy map for the measured system is shown in Fig. 6 for 628-nm illumination. No corrections are applied for dark current or flat-field response. The focus specification of better than 50% ensquared energy for a point source is easily met over most of the field of regard and fails prior to correction only in the center of CCD1's field of view. These measurements have an uncertainty of about 5%; sometimes, all the field of regard was within specification, sometimes there were minor deviations. The map changes very little as a function of temperature, verifying the design prediction of athermal behavior.

Distortions were mapped by projecting a HeNe laser spot sequentially to 256 positions per CCD and then calculating 32 coefficients (16 per axis) for a polynomial fit. Each CCD imager has its own set of coefficients. Table 5 shows the residual pixel errors in target viewing axes for the coefficients determined at telescope temperatures of +22°C and −65°C. In all cases, the errors are well below the 0.2-pixel data analysis error budget. To determine the sensitivity of the distortion map to temperature, the coefficients taken at +22°C were used to determine the residual pixel errors for the −65°C data. The results for three of the imagers are shown in the last column of Table 5. Although the *y* axis for CCD3 has an error greater than 0.2 pixel, the distortion has a low temperature dependence. The absolute positions, relative to an optical cube mounted on the telescope body, changed less than a pixel throughout testing, including a launch simulation vibration test sequence.

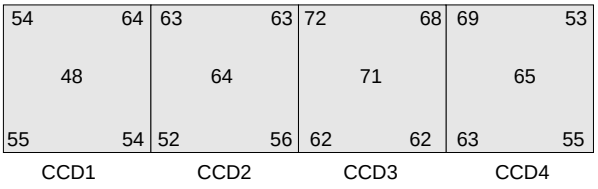

Figure 6. Ensquared energy map showing raw data prior to flat-field correction. The focal plane temperature was −42°C, and the telescope temperature was −35°C.

Flat-field uniformity was measured by placing a large integrating sphere in front of the telescope aperture. Three separate flat-field functions were noted: As predicted by the optical design, the steradiancy of pixels varied somewhat as a function of field position, there was a slight misalignment of a light shield over the focal plane, and the CCD had an inherent sensitivity pattern. Over the field of regard, the flat-field nonuniformity was about 12%, mostly due to the predictable steradiancy change.

Radiometric calibration accuracy was defined as the residual errors after compensating for the stable flat-field patterns and reference radiometer accuracy. Data were taken with the same large integrating sphere used for flat-field measurements. Data errors were dominated by equipment calibration accuracy, setup repeatability, and drift, rather than inherent sensor instabilities. The calibration variations had about 2.5% repeatability and are estimated to have absolute errors of <10%, well within the

Table 4. Calibration parameters and specifications.

Parameter	Specification
Focus	>50% ensquared energy
Distortion map	Correctable to 0.2 pixel
Flat-field uniformity	Stable
Radiometry	<20% calibration error for entrance aperture irradiance for CCD3
	0.5 visual magnitude elsewhere
Dark current	<100 electrons/pixel·s
Noise	<10 electrons rms at 0.4 s integration
BRDF	$<3 \times 10^{-3}$ at 1°, rolling off at the second power

Table 5. Telescope distortion mapping errors (*y* axis/*z* axis).

CCD	rms error at +22°C	rms error at −65°C	Wrong map errors
1	0.050/0.074	0.054/0.074	0.127/0.095
2	0.071/0.073	0.070/0.073	0.144/0.083
3	0.063/0.064	0.118/0.100	0.317/0.140
4	0.120/0.080	0.170/0.084	Not analyzed

Note: The errors are shown in pixels; they represent the differences between the measurements and the correction polynomial.

required 20%. Additional effort was not expended to refine the radiometric calibration process once the program requirements were surpassed.

Dark current and noise tend to be related in CCD camera systems. At a focal plane temperature of −42°C, which is the nominal operating temperature, the imagers had a dark current of 18 electrons per second per pixel, well within the allowed limit of 100 electrons per second. Noise, with the cover closed, was measured to be 6.9 electrons rms at a 0.4-s integration time. Noise was measured both as a temporal variation of a single pixel and as an area average in a single frame. Both methods gave the same results. Focal plane calibrations conducted prior to integration with the telescope showed that the SBV CCDs were capable of transferring charge packets as low as 10 electrons with no apparent loss. The charge transfer remained unchanged down to operating temperatures of −55°C, where the dark current, which acts as a "slim zero," was less than 2 electrons per pixel. The focal planes were screened for pocket density (pockets are electron traps in the imager that cause a variety of temporal and spatial imaging distortions). No pockets greater than 100 electrons were noted on any imager, and none were detectable on CCD3, the boresite imager.

The last calibration parameter was the bidirectional reflectance distribution function (BRDF), a measure of the scattering mechanisms inside the telescope. The telescope was delivered meeting its specification. Figure 7 shows the BRDF measurement history of the telescope over nearly 2 years, plotted as the sensitivity of the SBV sensor at two different tangent angles above a fully illuminated Earth disk. The BRDF seems to be very slowly degrading, probably due to minor particle buildup. Sensitivity is calculated from measured BRDF data and plotted in Fig. 7 as the minimum-diameter specular sphere detectable with a signal-to-noise ratio of 6.0 at both 100 and 350 km above the Earth tangent point. Smaller diameters indicate better detection sensitivity, corresponding to better rejection of the sunlight reflected from the Earth. The roll-off is faster than expected, allowing the sensor to meet its performance requirements, even with some additional contamination. The telescope has not been cleaned since delivery from SSG; we believe that the good level of cleanliness is due to strict adherence to contamination control procedures and to design decisions made with contamination control in mind.

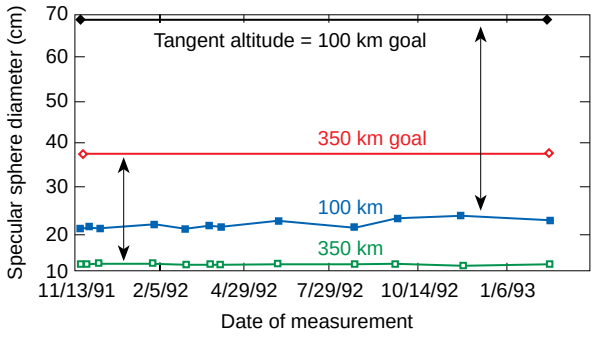

Figure 7. Calculated minimum detectable low-altitude target size, shown against performance goals for targets at 100 km and 350 km above Earth tangent point. The sphere reflectivity is 0.8, and the detection signal-to-noise ratio is 6.0.

End-to-End Testing

With a system as complex as the SBV sensor, there is always the concern that a critical parameter has been missed and that the sensor will not work properly. Ideally, the sensor would be brought to an observatory where it could operate looking at real scenes containing clutter (stars) and moving objects (satellites). The risk of contaminating the telescope forced us to reject this idea. To simulate a real observation, MIT/LL assembled an optical scene generator to project images into the telescope. A block diagram of the end-to-end test setup is shown in Fig. 8.

A series of complex frame sets were generated by a Vaxstation and loaded into a Tektronix high-resolution video monitor. These scenes contained stationary objects simulating stars and moving objects simulating satellites. The scenes had variable star brightnesses and several different satellite motions. The monitor images were projected through a collimator into the SBV telescope. After alignment to a CCD, the frame sets were synchronized to the SBV camera's timing using test port signals. The resulting images were collected by the camera and sent to the signal processor. The results were checked against predictions.

The flight hardware detected all objects and sent correct message types to the ground data analysis system. Just one problem was found: The metric positions of the simulated stars were in error. This problem was traced to distortions in the scene generator, both static and dynamic. The test was repeated for the remaining three CCDs in the SBV focal plane, and no other problems were found.

With calibration complete, the remaining tasks were to integrate the SBV sensor into the MSX spacecraft at APL and run through the spacecraft-level testing. The electronics were integrated successfully in March 1993, and the telescope was integrated in May 1994.

CURRENT STATUS

The SBV flight sensor program was initiated in April 1989. All flight hardware has been built and tested, meeting or exceeding requirements. The electronic units integrated into the MSX spacecraft in March 1993 have been tested periodically to verify that

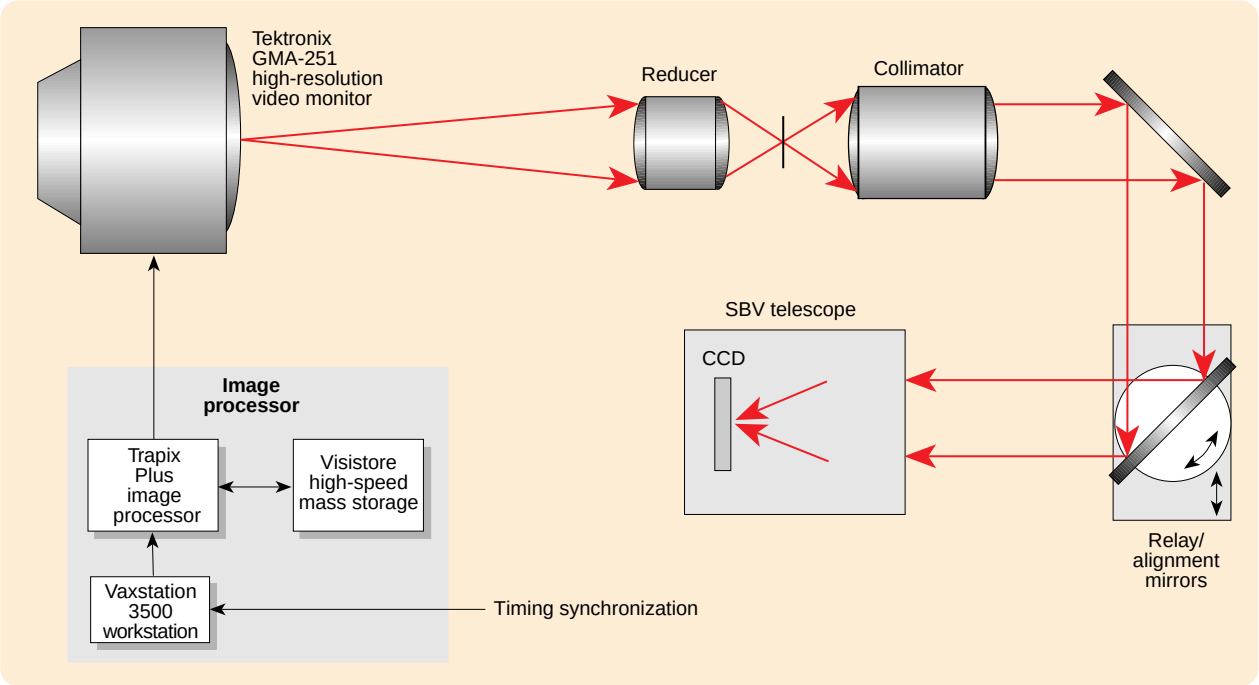

Figure 8. End-to-end test block diagram.

all functions continue to work. The telescope integration in May 1994 followed integration of the Spatial Infrared Imaging Telescope III. A single cold test was run during thermal vacuum testing at Goddard Space Flight Center, validating the SBV thermal design. Periodic warm testing since then has indicated no change in instrument parameters.

REFERENCES

[1] Dyjak, C. P., and Harrison, D. C., "Space-Based Visible Surveillance Experiment," *SPIE Proc.* **1479**, Surveillance Technologies, pp. 42–56 (1991).
[2] Mill, J. D., O'Neill, R. R., Price, S., Romick, G. J., Uy, O. M., and Gaposchkin, E. M., "Midcourse Space Experiment: Introduction to the Spacecraft, Instruments and Scientific Objectives," *J. Spacecr. Rockets* **31**(5), 900–907 (1994).
[3] Wang, D., Wong, C., and Gardner, R., "Space-Based Visible All-Reflective Stray Light Telescope," *SPIE Proc.* **1479**, Surveillance Technologies, pp. 57–70 (1991).
[4] Burke, B. E., Mountain, R. W., Daniels, P. J., and Harrison, D. C., "420 × 420 Charge-Coupled Device Imager and Four-Chip Focal Plane," *Opt. Eng.* **26**(9), 890–896 (1987).
[5] Burke, B. E., Mountain, R. W., Harrison, D. C., Bautz, M. W., Doty, J. P., et al, "An Abuttable CCD Imager for Visible and X-Ray Focal Plane Arrays," *IEEE Trans. Electron Devices* **ED-38,** 1069–1076 (1991).
[6] Chu, P., *Efficient Detection of Small Moving Objects*, Lincoln Laboratory Technical Report TR-846, DTIC AD-A213314, Lexington, MA (21 Jul 1989).
[7] Anderson, J. C., Downs, G. S., and Trepagnier, P. C., "A Signal Processor for Space-Based Visible Sensing," *SPIE Proc.* **1479**, Surveillance Technologies, pp. 78–92 (1991).
[8] Harrison, D. C., and Chow, J. C., "Space-Based Visible Sensor on MSX Satellite," *SPIE Proc.* **2217**, Aerial Surveillance Sensing Including Obscured and Underground Object Detection, pp. 377–387 (1994).

ACKNOWLEDGMENTS: The SBV program would not have been a success without the cooperation and hard work of many at MIT/LL. In particular, we wish to acknowledge the invaluable guidance and advice of the late Charles P. Dyjak, who was instrumental in developing the basic concept of a moderate-size space-based space surveillance experiment. We also wish to thank SSG, Inc., Waltham, Massachusetts, for a fine telescope that meets all of our requirements; SCI, Inc., Huntsville, Alabama, for designing a compact, reliable computer to control SBV; and Gulton Data Systems, Albuquerque, New Mexico, for providing a power subsystem better than our specifications. This work was sponsored by the Air Force Space and Missile Systems Center, Space Based Infrared Systems Program Office, under Air Force contract F19628-95-C-0002, and the MSX mission is sponsored by the Ballistic Missile Defense Organization.

THE AUTHORS

DAVID C. HARRISON received a B.S.E.E. from the Massachusetts Institute of Technology in 1965. He is a senior staff member at MIT Lincoln Laboratory, where he has been devising electro-optical and other imaging systems for more than 30 years, concentrating on slow-scan applications of CCDs for the past 17 years. He was the project engineer for the HRI, an X-ray imager that was successfully flown on the Einstein and Rosat spacecraft and is currently planned to be used on AXAF. At Lincoln Laboratory, Mr. Harrison has been designing cameras and focal planes for a variety of space surveillance applications, both ground and space based. He is the architect of many of Lincoln Laboratory's high-performance imagers and is the systems engineer for the SBV sensor. His e-mail address is harrison@LL.MIT.EDU.

JOSEPH C. CHOW received a B.S.E.E. from National Taiwan University in 1965, and M.S. and Ph.D. degrees from Harvard in 1967 and 1971, respectively. He was an Assistant Professsor at Wayne State University before joining MIT Lincoln Laboratory in 1972, where he is the group leader of the Advanced Sensors and Systems Group and the program manager for the SBV project. Dr. Chow has worked on air traffic control, ballistic missile defense countermeasures and discrimination, space surveillance, space-based radar, and space-based electro-optical technology programs. From 1979 to 1982, Dr. Chow was stationed at Kwajalein Missile Range as leader of the TRADEX and ALTAIR radars. His e-mail address is chow@LL.MIT.EDU.